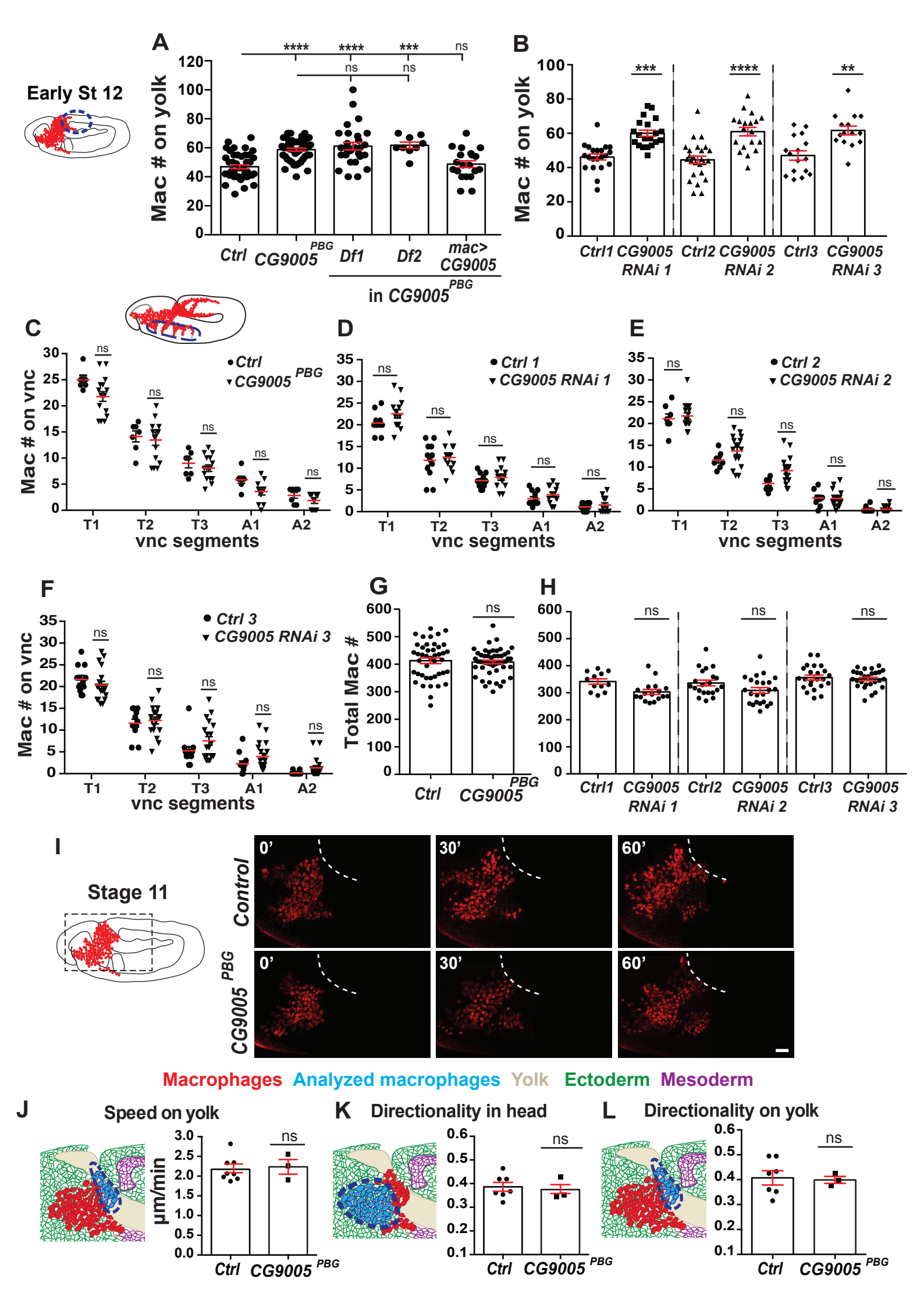
A
Early St 12
Mac # on yolk
Ctrl
CG9005 PBG
Df1
Df2
mac> CG9005 in CG9005 PBG
B
Mac # on yolk
Ctrl1
CG9005 RNAi 1
Ctrl2
CG9005 RNAi 2
Ctrl3
CG9005 RNAi 3
C
Mac # on vnc
Ctrl
CG9005 PBG
vnc segments
D
Ctrl 1
CG9005 RNAi 1
E
Ctrl 2
CG9005 RNAi 2
F
Ctrl 3
CG9005 RNAi 3
G
Total Mac #
H
I
Stage 11
Control
CG9005 PBG
0'
30'
60'
Macrophages
Analyzed macrophages
Yolk
Ectoderm
Mesoderm
J
Speed on yolk
µm/min
K
Directionality in head
L
Directionality on yolk

Figure S1 related to Figure 1: *CG9005^{PBG}* mutant macrophages migrate normally within the head and along the vnc. Fig S1A-B. Quantification of macrophages on the yolk in fixed early Stage 12 embryos shows a significant increase in (**A**) the *P{GT1}CG9005^{BG02278}* P element mutant (*CG9005^{PBG}*) and in (**B**) lines expressing each of the CG9005 RNAis in macrophages compared to the control. (**A**): control n=43, mutant n=50, mutant/*Df1* n=28, mutant/*Df2* n=9, rescue=20; p<0.0001 for control vs mutant, p=0.99 for control vs rescue, p=0.001 for mutant vs rescue. (**B**): control 1 n=21, CG9005 *RNAi 1* n=20, p=0.0002; control 2 n=25, CG9005 *RNAi 2* n=19, p<0.0001; control 3 n=16, CG9005 *RNAi 3* n=15, p=0.001). **Fig S1C-F.** Macrophage quantification in ventral nerve cord (vnc) segments reveals no significant difference in macrophage migration along the vnc between *CG9005^{PBG}* mutant (n=15) and control embryos (n=7, p>0.05) or *srpHemo>CG9005 RNAi* embryos compared to the controls (control 1 n=8, CG9005 *RNAi 1* n=13, p=0.25; control 2 n=8, CG9005 *RNAi 2* n=16, p=0.5; control 3 n=8, CG9005 *RNAi 3* n=16, p>0.99). **Fig S1G-H.** Quantification of the total macrophage number reveals no significant difference between the control (n=43) and *CG9005^{PBG}* mutant embryos (n=50, p=0.69), or the control and *srpHemo>CG9005 RNAi* embryos (control 1 n=12, *CG9005 RNAi 1* n=17, p=0.9; control 2 n=27, *CG9005 RNAi 2* n=19, p=0.84; control 3 n=23, *CG9005 RNAi 3* n=27, p=0.16). **Fig S1I.** Stills from two-photon movies of control and *CG9005^{PBG}* mutant embryos, showing macrophages migrating starting at Stage 10 from the head towards the germband. Elapsed time indicated in minutes. The germband edge (white dotted line) was detected by yolk autofluorescence. **Fig S1J-L.** Quantification of migration parameters from two-photon live imaging of macrophages. **Fig S1J.** Macrophages on the yolk sac in the *CG9005^{PBG}* mutant reach the germband with a similar speed to control macrophages. Speed: control and mutant=2.2 μm/min; movie #: control=8, mutant=3; track #: control=373, mutant=124, p=0.78. **Fig S1K-L.** Macrophage directionality (**K**) in the head or (**L**) on the yolk sac shows no change in the *CG9005^{PBG}* mutant compared to the control. Head directionality: control=0.39, mutant=0.37, p=0.74; yolk sac directionality: control=0.40, mutant=0.39, p=0.86. Macrophages analyzed in **A-L** were labeled with *srpHemo-H2A::3xmCherry* to visualize nuclei. In schematics, macrophages are shown in red and analyzed macrophages in light blue, the ectoderm in green, the mesoderm in purple, and the yolk in beige. Throughout this work embryos were staged for imaging and quantification based on germband retraction away from the anterior of less than 29% for stage 10, 29%–31% for stage 11, and 35%–40% for stage 12. In all figures histograms show mean±SEM, ns=p>0.05, *p<0.05, **p<0.01, ***p<0.001, ****p<0.0001. One-way ANOVA with Tukey for (**A**) and unpaired t test for (**B**-**H**) and (**J**-**L**).

Figure. S2

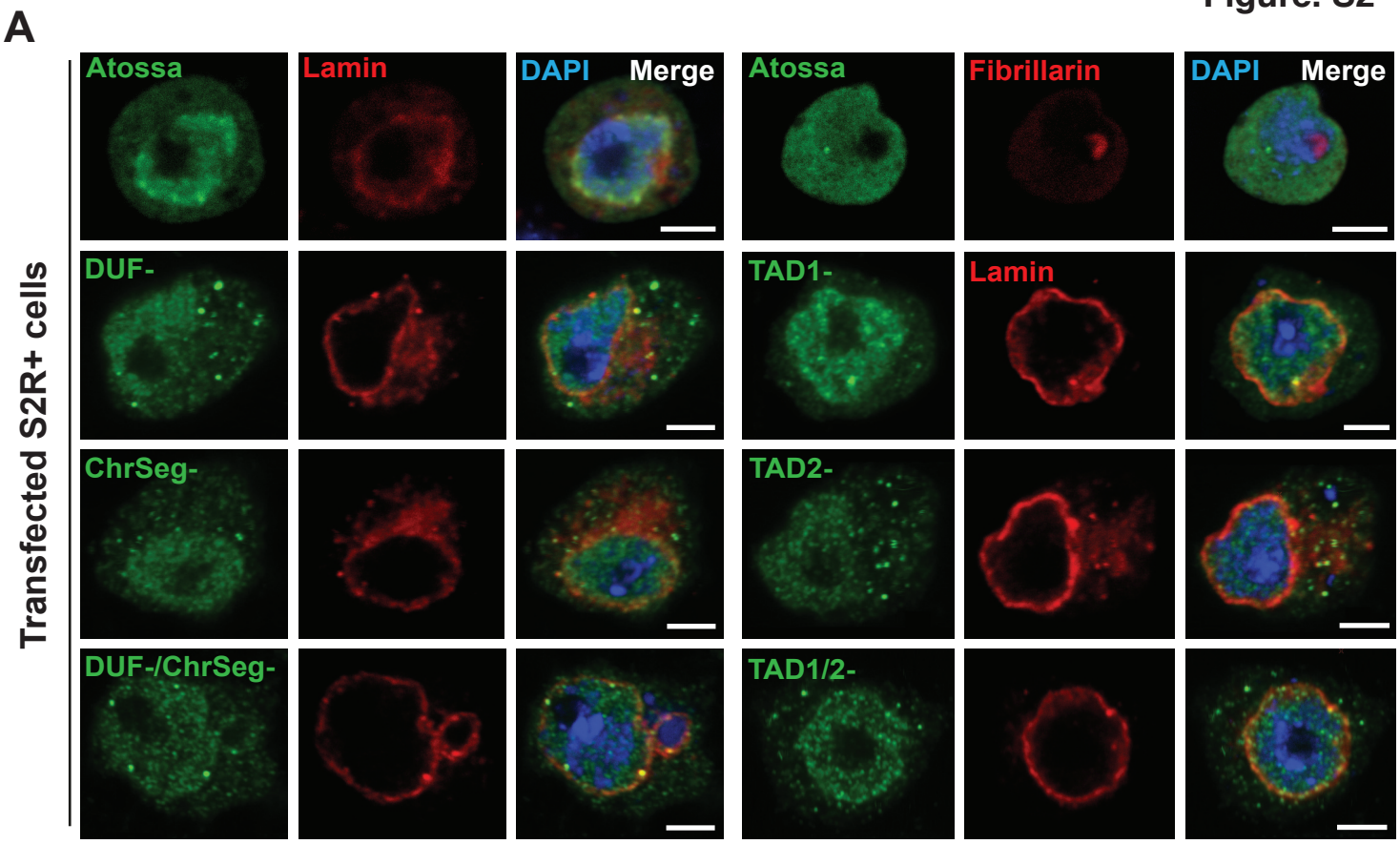
A
Transfected S2R+ cells
Atossa
Lamin
DAPI
Merge
Atossa
Fibrillarin
DAPI
Merge
DUF-
TAD1-
Lamin
ChrSeg-
TAD2-
DUF-/ChrSeg-
TAD1/2-

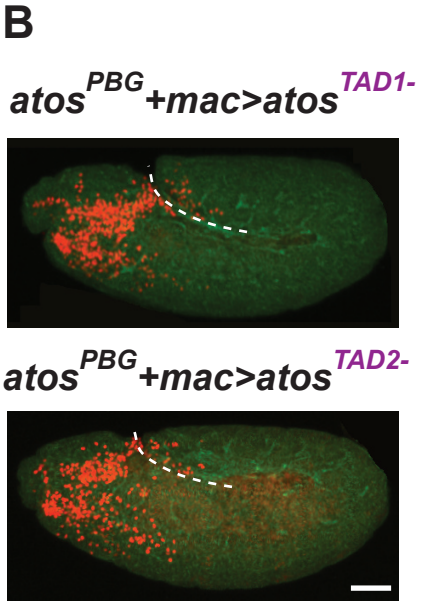
B
atos PBG +mac>atos TAD1-
atos PBG +mac>atos TAD2-

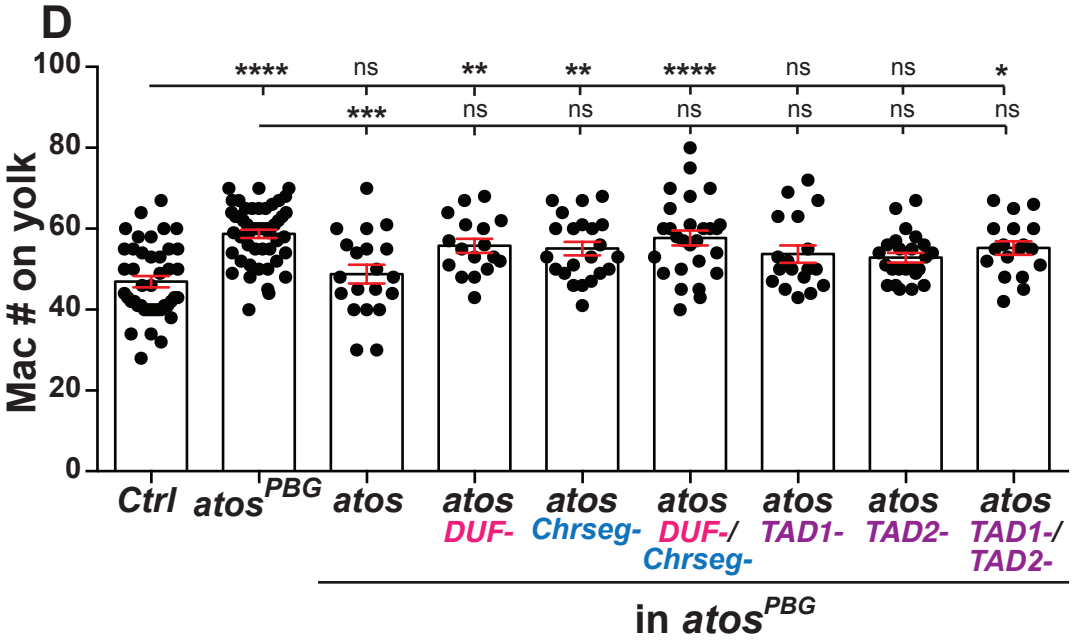
D
Mac # on yolk
Ctrl
atos PBG
atos
atos DUF-
atos Chrseg-
atos DUF-/ Chrseg-
atos TAD1-
atos TAD2-
atos TAD1-/ TAD2-
in atos PBG

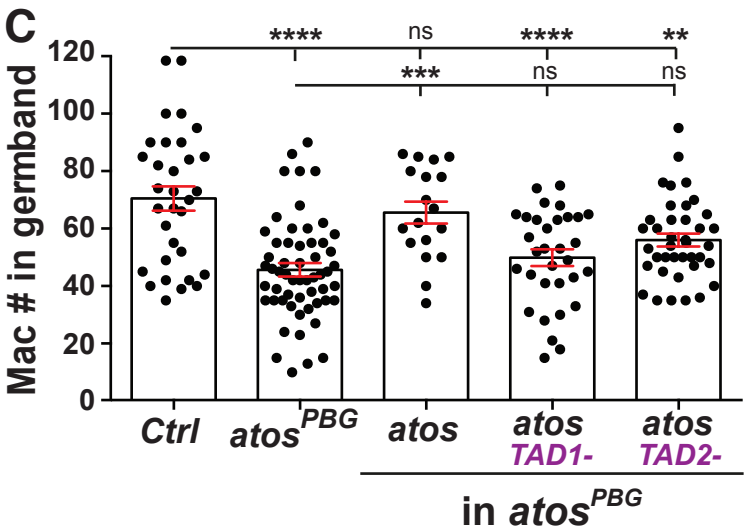
C
Mac # in germband
Ctrl
atos PBG
atos
atos TAD1-
atos TAD2-
in atos PBG

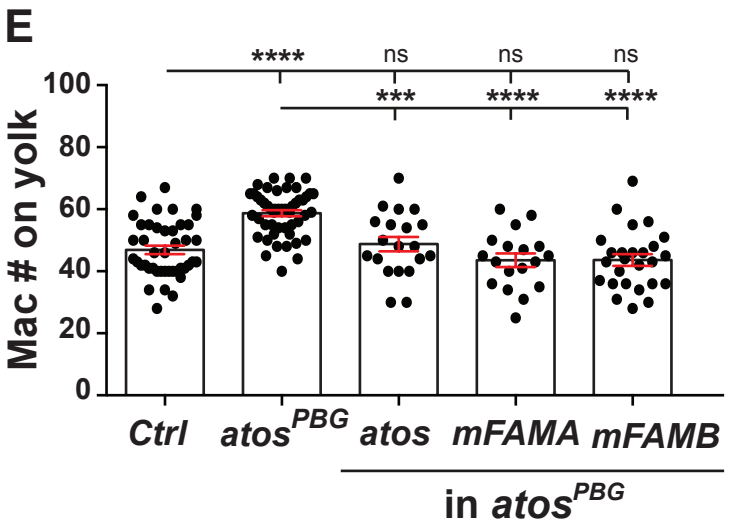
E
Mac # on yolk
Ctrl
atos PBG
atos
mFAMA
mFAMB
in atos PBG

Figure S2 related to Figure 2. Atos's TAD domains are essential in macrophages for their tissue infiltration. Fig. S2A. S2R+ cells were transfected with wild type Atos or forms lacking the indicated domains. HA tagged Atos (green), the nuclear membrane marker Lamin (red) and the nucleolar marker Fibrillarin (red) were visualized with antibodies, and nuclear DNA with DAPI (blue). All forms of Atos are expressed under direct control of the *srpHemo* promoter. **Fig S2B.** Representative confocal images of Stage 12 embryos from $atos^{PBG}$ mutants expressing Atos lacking either TAD1 or 2 in macrophages from the *srpHemo* promoter. Macrophages (red) were visualized with *srpHemo-H2A::3xmCherry* expression and the embryo outlines with phalloidin staining to detect actin (green). **Fig S2C.** Quantification shows that deletion of TAD1 or 2 blocks Atos's ability to rescue the germband migration defect of Stage 12 $atos^{PBG}$ mutant embryos upon expression in macrophages. Control n=32, mutant n=56, WT rescue n=18, $TAD1^-$ n=32, $TAD2^-$ n=39. For control vs WT rescue $p>0.99$, for control vs $TAD1^-$ rescue $p<0.0001$, and for control $TAD2^-$ rescue $p=0.003$. **Fig S2D.** Quantification in fixed early Stage 12 embryos shows a significant increase in the number of macrophages on the yolk in the $atos^{PBG}$ mutant and $atos^{PBG}$ expressing forms of *atos* lacking either DUF4210, ChrSeg, both DUF4210 and ChrSeg, or TAD1 and TAD2 compared to control embryos and $atos^{PBG}$ embryos expressing WT Atos. Control n=43, *atos* mutant n=50, WT *atos* rescue n=20, $DUF4210^-$ rescue n=17, $ChrSeg^-$ rescue n=22, $DUF4210^-/ChrSeg^-$ rescue n=27, $TAD1^-$ rescue n=18, $TAD2^-$ rescue n=24, $TAD1^-/TAD2^-$ rescue n=18. For control vs *atos* mutant $p<0.0001$, for control vs WT rescue $p>0.99$, for control vs. other rescues expressing *atos* lacking conserved motifs $p>0.1$. **Fig S2E.** Quantification shows a similar number of macrophages on the yolk in fixed early Stage 12 $atos^{PBG}$ mutant embryos which express *mFAM214A* or *mFAM214B* in macrophages compared to the control. Control n=43, mutant n=50, WT rescue n=20, *mFAM214A* rescue n=18, *mFAM214B* rescue n=26. For control vs $atos^{PBG}$ $p=0.93$, for control vs *mFAM214A* rescue $p=0.65$, for control vs *mFAM214B* rescue $p=0.56$, for $atos^{PBG}$ mutant vs $atos^{PBG}$, *mFAM214A* and *mFAM214B* rescues $p<0.0001$. One-way ANOVA with Tukey for (**C**-**E**). Scale bars: 3 µm in (**A**), 50 µm in (**B**).

Figure. S3

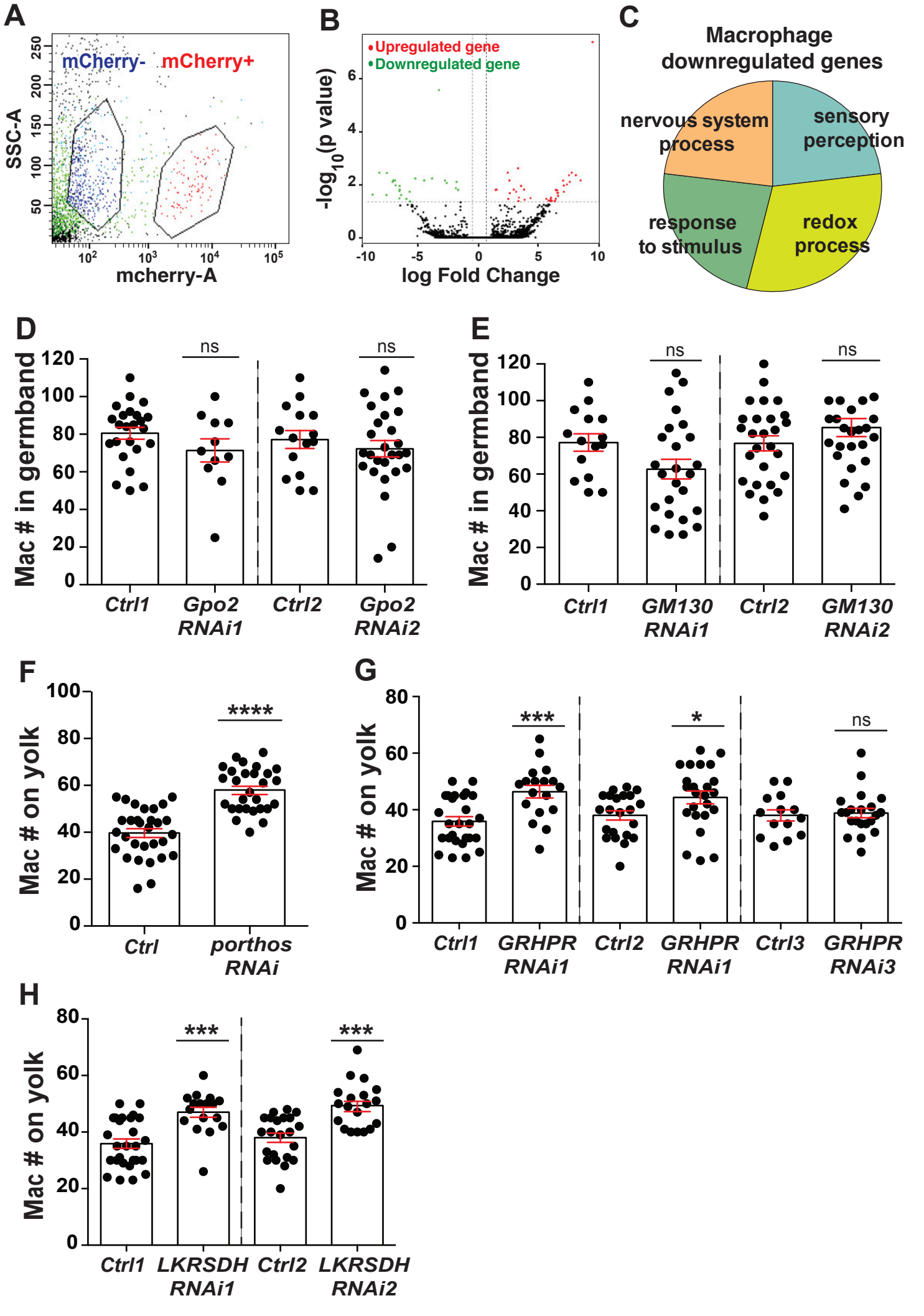
A
mCherry-
mCherry+
SSC-A
mcherry-A
B
Upregulated gene
Downregulated gene
-log10(p value)
log Fold Change
C
Macrophage downregulated genes
nervous system process
sensory perception
response to stimulus
redox process
D
Mac # in germband
ns
Ctrl1
Gpo2 RNAi1
Ctrl2
Gpo2 RNAi2
E
Mac # in germband
ns
Ctrl1
GM130 RNAi1
Ctrl2
GM130 RNAi2
F
Mac # on yolk
****
Ctrl
porthos RNAi
G
Mac # on yolk
***
*
ns
Ctrl1
GRHPR RNAi1
Ctrl2
GRHPR RNAi1
Ctrl3
GRHPR RNAi3
H
Mac # on yolk
***
***
Ctrl1
LKRSDH RNAi1
Ctrl2
LKRSDH RNAi2

Figure S3 related to Figure 3. Macrophage transcriptome analysis reveals that Atos targets participate in signaling, cell communication and ion transport.

Fig S3A. FACS plot of Side Scatter (SSC) vs. mCherry fluorescence signal in macrophages obtained from embryos expressing *srpHemo-3xmCherry*. The two populations are sorted as mCherry marker + (red) and – (blue) cells. **Fig S3B.** Genes expressed differentially in analysis of RNA sequencing data from macrophages from the $atos^{PBG}$ mutant compared to the control are shown in a volcano plot graphing the $\log_{10}$ of the P value against the log fold change (FC) of the mean normalized expression levels. Each point represents the average value of one gene's expression from four replicate experiments. Dotted vertical lines indicate a $\log_{10}$ fold change ≥ 1 and the dotted horizontal line a *P* value of ≤ 0.05. Statistically significant up- and down-regulated genes are reported as red and green dots, respectively. **Fig S3C.** Gene ontology (GO) analysis of downregulated genes from $atos^{PBG}$ mutant macrophages compared to the control shows that theses genes are involved in oxidation-reduction processes, stress responses as well as the nervous system. **Fig S3D-E.** Quantification in fixed early Stage 12 embryos reveals that knockdown by two different RNAis of (**D**) *Glycerophosphate oxidase 2* (*Gpo2*, *CG2137* or (**E**) *Golgi matrix protein 130 kD* (*GM130*, CG11061) did not change the macrophage number within the germband compared to their controls. For (**D**) control 1 n=24, *Gpo2 RNAi 1* (VDRC 41234) n=11, p=0.26; control 2 n=15, *Gpo2 RNAi 2* (VDRC 68145) n=27, p=0.38. For (**E**) control 1 n=15, *GM130 RNAi 1* (VDRC 330284) n=25, p=0.14; control 2 n=27, *GM130 RNAi 2* (VDRC 64920) n=20, p=0.34. **Fig S3F-H.** Quantification reveals that expression of RNAis against *porthos, GR/HPR,* and *LKR/SDH* in macrophages leads to a significant increase in macrophage numbers on the yolk in fixed early Stage 12 embryos compared to their controls. For (**F**) control n=30, *porthos* RNAi n=28, p<0.0001. For (**G**) control 1 n=27, *dGR/HPR RNAi 1* (VDRC 44653) n=18, p=0.0003; control 2 n=22, *dGR/HPR RNAi* 2 (VDRC 107680) n=24, p=0.04; control 3 n=14, *dGR/HPR RNAi 3* (VDRC 64652) n=21, p=0.7. For (**H**) control 1 n=27, *dLKR/SDH RNAi 1* (VDRC 51346) n=17, p=0.0002; control 2 n=22, *dLKR/SDH RNAi 2* (VDRC 109650) n=19, p=0.0004. Unpaired t test for (**D**-**H**).

Figure. S4

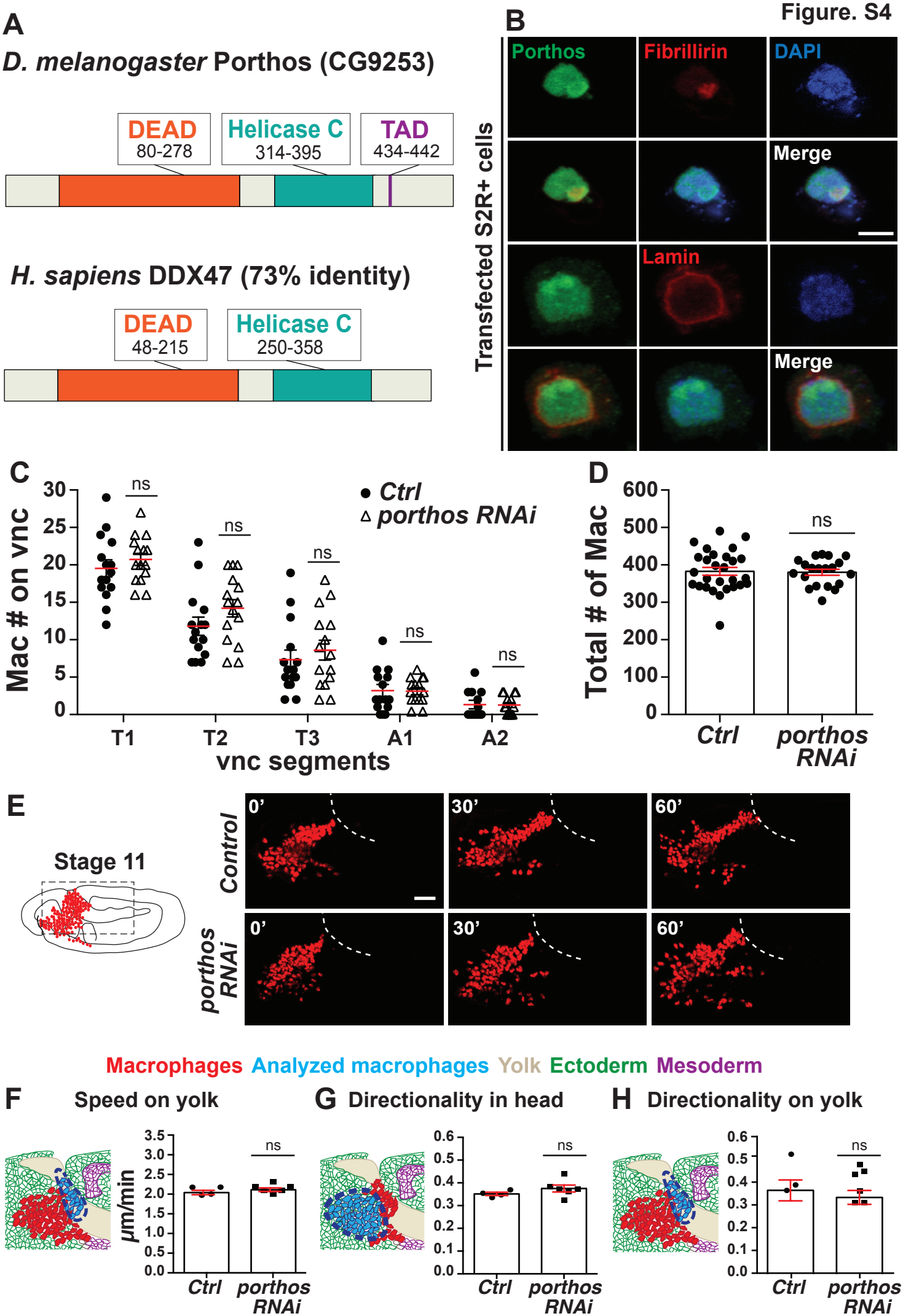
A
D. melanogaster Porthos (CG9253)
DEAD
80-278
Helicase C
314-395
TAD
434-442
H. sapiens DDX47 (73% identity)
DEAD
48-215
Helicase C
250-358
B
Transfected S2R+ cells
Porthos
Fibrillirin
DAPI
Merge
Lamin
Merge
C
Mac # on vnc
Ctrl
porthos RNAi
ns
T1
T2
T3
A1
A2
vnc segments
D
Total # of Mac
Ctrl
porthos RNAi
E
Stage 11
Control
porthos RNAi
0'
30'
60'
Macrophages
Analyzed macrophages
Yolk
Ectoderm
Mesoderm
F
Speed on yolk
µm/min
G
Directionality in head
H
Directionality on yolk

Figure S4 related to Figure 4. Downregulation of *porthos* recapitulates the *atos* mutant phenotype.

Fig S4A. Deduced protein structure of Porthos (CG9253). Porthos contains two conserved motifs, a DEAD motif (Asp-Glu-Ala-Asp) and a Helicase C domain, as well as a predicted transactivation domain (TAD). *Drosophila* Porthos shows 71% identity and 84% similarity to its human ortholog, DDX47. **Fig S4B.** Porthos (green) in S2R+ cells transfected with *UAS-porthos::HA* and *srpHemo-Gal4*, and stained for the nuclear membrane marker Lamin (red), colocalizes with the staining for the nucleolar marker Fibrillarin (red), and DAPI (blue). **Fig S4C-D.** Quantification of macrophage numbers in fixed Stage 12 embryos. (**C**) Expression of *porthos RNAi* in macrophages has no effect in their numbers on (**C**) the vnc or (**D**) in the whole embryo compared to the control. For (**C**) control n=15, *porthos RNAi* n=15, p>0.35. For (**D**) control n=28, *porthos RNAi* n=20, p=0.85. **Fig S4E.** Stills from two-photon movies of the migration of macrophages labeled with *srpHemo-H2A::3xmCherry* in control embryos and in those expressing *porthos RNAi* in macrophages. Macrophages from both genotypes have a similar (**F**) directionality in the head, and (**G**) speed and (**H**) directionality on the yolk sac, to control macrophages. Speed on yolk sac: control=2.10 μm/min, *porthos RNAi*=2.15 μm/min; p=0.35; movie #: control n=4, *porthos RNAi* n=6; track #: control n=104, *porthos RNAi* n=168. Directionality in head: control n=0.35, *porthos RNAi* n=0.37; p=0.27; movie #: control n=4, *porthos RNAi* n=6. Directionality on yolk: control=0.42, *porthos RNAi*=0.39; p=0.58; movie #: control n=3, *porthos RNAi* n=6. Unpaired t test for (**C**), (**D**), and (**F-H**). Scale bar is 5 μm in (**B**) and 30 μm in (**E**).

Figure. S5

A

Biological function	Gene symbol	Description of Porthos targets	Vertebrate ortholog
DNA regulation, Transcription	CG11403	DNA DEAD/H box helicase 11	Ddx11
	CG11335	Lysyl oxidase-like 1 (Loxl1), euchromatinization	Loxl2
	CG10694	nucleotide-excision repair	Rad23a
	CG12659	Chromatin remodeling	Ino80c
	CG5441	taxi, transcription factor	Atoh1
	CG13005	Zinc finger protein 839, transcription factor	Zfp839
	CG7963	Zinc finger C2H2 transcription factor	Gm14322
	CG8021	SLIRP2, mRNA processing	Slirp
	CG8159	Regulation of transcription	Plag1
	CG11456	Regulation of transcription by RNA polymerase II	Plagl2
	CG10654	Regulation of transcription by RNA polymerase II	J23Rik
	CG31626	Regulation of transcription by RNA polymerase II	Pou2af1
	CG12442	wuc, regulation of transcription by RNA polymerase II	Lin52
	CG12320	A1 cistron-splicing factor, AAR2	Aar2
	CG12938	U7 snRNA-associated Sm-like protein LSm10	Lsm10
	CG7637	snRNA/rRNA pseudouridine synthesis	Nop10
RNA translation	CG15693	RpS20, ribosomal small protein S20	Rps20
	CG3997	RpL39, ribosomal large protein L39	Rpl39l
	CG30425	RpL41, ribosomal large protein L41	NF
	CG4061	Rtca, RNA 3'-terminal phosphate cyclase	Rtca
	CG18643	Dtd, D-aminoacyl-tRNA deacylase, tRNA metabolic process	Dtd1
Protein degradation	CG8272	SCF-dependent proteasomal ubiquitin-dependent proteolysis	Lrrc29
	CG14260	Proteasomal ubiquitin-dependent proteolysis	NF
	CG31807	Ubiquitin-protein transferase	Rfwd3
	CG8419	Ubiquitin-protein transferase	Trim45
	CG32847	Ubiquitin-protein ligase	Rnf185
	CG5001	Chaperone/unfolded protein binding	Dnajb5
	CG2046	Proteasome assembly chaperone 1	Psmg1
	CG6972	Desumoylating isopeptidase 1	Desi1
Immune cell response	CG2723	ImpE3, Ecdysone-inducible gene E3	NF
	CG1367	Cecropin A2, activity against Gram-negative bacteria	NF
	CG10794	Diptericin B, activity against Gram-negative bacteria	NF
	CG16712	IM33 peptide against systemic microbial infection	Eppin
	CG33493	Antibacterial humoral response	Ndufa5

B

Biological function	Gene symbol	Description of Porthos targets	Vertebrate ortholog
Signal transduction	CG1279	reticulon 2, ER organization and function	Rtn1
	CG5417	Srp14, protein targeting to ER	Srp14
	CG12843	Tetraspanin 42Ei, Integrin signaling	Cd63
	CG5657	Sarcoglycan β, negative regulator of EGFR pathway	Sgcb
	CG3302	Corazonin, a G-protein-coupled receptor	NF
	CG42366	Mitogen-activated protein kinase	NF
	CG8767	Mos oncogeneactivates the MAPK cascade	Mos
	CG9336	positive regulation of voltage-gated K+ channel	NF
	CG3504	inaD, fast light-induced signaling	Lnx1
	CG7916	Haemolymph juvenile hormone binding	NF
	CG18188	Damm, caspase family of cysteine proteases	Casp6
	CG9470	Metallothionein A, metal ion homeostasis	Mt1
	CG3227	insensitive, corepressor for the product of Su(H)	NF
	CG17479	Sphingosine kinase 1, regulates cell division/traffiking	NF
	CG17962	Z600, a mitotic inhibitor	NF
	CG10861	Autophagy-related 12	Atg12
	CG14937	G2/M transition of mitotic cell cycle	NF
	CG32812	negative regulation of phosphatase activity	Chp1
	CG31391	negative regulation of phosphatase activity	Ppp1r36
Transport	CG17137	Porin2, voltage-dependent anion channel 1	Vdac1
	CG7912	Sulfate transport and transmembrane transport	Slc26a11
	CG18345	Trpl, transient receptor potential-like	Trpc5
	CG32069	ER to Golgi vesicle-mediated transpor	Ier3ip1
	CG11703	Sodium:potassium-exchanging ATPase	Atp1b1
	CG5421	H(+)-transporting two-sector ATPase	Atp6ap1l
Cell-cell interaction	CG13664	Cadherin 96Cb, control of cell adhesion	Cdh6
	CG16719	Regulation of cytoskeleton organization	Spef1
	CG5987	TTLL6B, microtubule cytoskeleton organization	Ttll6
	CG4537	Cytoplasmic microtubule organization	Cript
	CG7802	Neyo, regulation of cell shape/apical constriction	NF
	CG12408	Troponin C isoform 4, control of muscle contraction	Calm4
	CG8121	Pasiflora 2 (pasi2), endothelial barrier function	NF
	CG5458	Radial spoke head protein 1, axoneme assembly	Rsph1
	CG31020	Sanpodo, cell division/cell fate determination	NF
	CG31801	Mst36Fa, spermatogenesis	NF

Figure S5 related to Figure 5. Porthos increases the translation of a subset of mRNAs.

Fig 5SA-B. Other target mRNAs downregulated in *porthos KD* cells are involved in gene regulation and RNA processing, mRNA translation, cellular transport, cell signaling, cell-cell interactions, immune responses, and protein degradation. NF: Not Found.

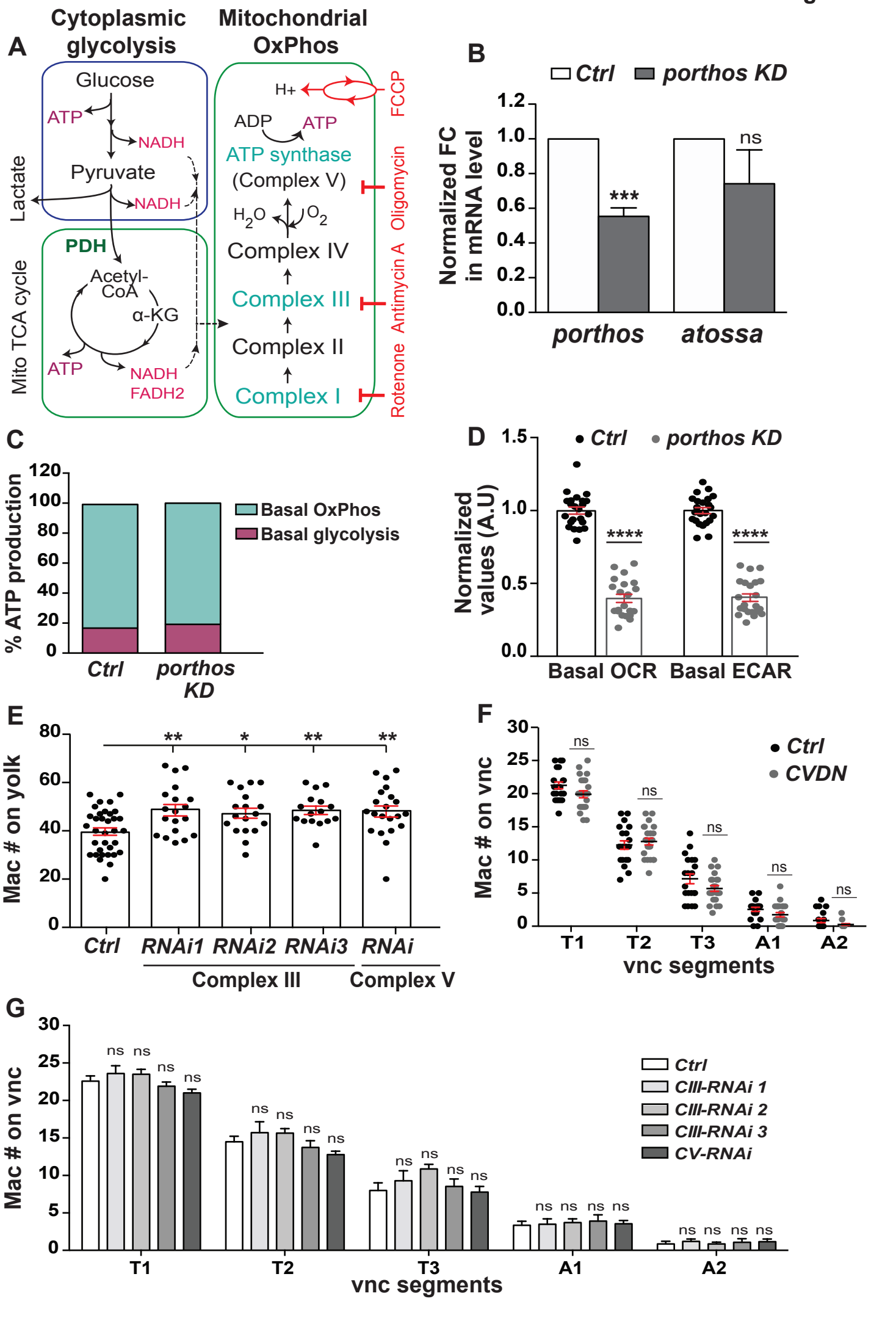
A
Cytoplasmic glycolysis
Mitochondrial OxPhos
Glucose
ATP
NADH
Pyruvate
NADH
Lactate
PDH
Acetyl-CoA
α-KG
ATP
NADH
FADH2
Mito TCA cycle
H+
FCCP
ADP
ATP
ATP synthase
(Complex V)
Oligomycin
H2O
O2
Complex IV
Complex III
Antimycin A
Complex II
Complex I
Rotenone
B
Ctrl
porthos KD
Normalized FC in mRNA level
1.2
1.0
0.8
0.6
0.4
0.2
0.0
***
ns
porthos
atossa
C
% ATP production
120
100
80
60
40
20
0
Basal OxPhos
Basal glycolysis
Ctrl
porthos KD
D
Ctrl
porthos KD
Normalized values (A.U)
1.5
1.0
0.5
0.0
****
****
Basal OCR
Basal ECAR
E
Mac # on yolk
80
60
40
20
0
**
*
**
**
Ctrl
RNAi1
RNAi2
RNAi3
RNAi
Complex III
Complex V
F
Mac # on vnc
30
25
20
15
10
5
0
Ctrl
CVDN
ns
T1
T2
T3
A1
A2
vnc segments
G
Mac # on vnc
30
25
20
15
10
5
0
Ctrl
CIII-RNAi 1
CIII-RNAi 2
CIII-RNAi 3
CV-RNAi
ns
T1
T2
T3
A1
A2
vnc segments

Figure S6 related to Figure 6. Depletion of *atos* or *porthos* causes impairment in mitochondrial metabolic activity, reduced ATP production, and a deficiency in macrophage tissue invasion.

Fig S6A. Schematic indicating the specific inhibitors (in red at right) used to block the function of mitochondrial OxPhos components. The glycolysis, TCA cycle, and mitochondrial respiratory chain in eukaryotic cells are shown. **Fig S6B.** Graph shows relative *porthos* and *atos* mRNA levels (± SEM) in *porthos KD* S2R+ cells measured by qPCR from at least three independent experiments. The data are normalized to results for the internal control gene RpS20. *Porthos KD* S2R+ cells contain 56% of normal *porthos* mRNA levels and display a slight statistically insignificant decrease in *atos* mRNA levels. t-test was used followed by Sidak's correction. Control n=6, *porthos* n=6, p= 0.0002, *atos* n=3, p=0.09. **Fig S6C.** The contribution of basal OxPhos ATP production rate and glycolytic ATP production rate were calculated. The plot shows that both wild-type and *porthos KD* S2R+ cells utilize OxPhos respiration as the predominant bioenergetic pathway to produce ATP in these cells. Porthos depletion produced no increase in the relative utilization of glycolysis. **Fig S6D.** The relative basal values of the Oxygen Consumption rate (OCR), as a marker of OxPhos, and Extracellular Acidification Rate (ECAR), as an indication of glycolysis, in control and *porthos KD* S2R+ cells are plotted. Basal respiration rate is calculated before the addition of antimycin A. **Fig S6E.** Quantification in fixed early Stage 12 embryos shows a significant increase of macrophages on the yolk upon the expression in macrophages of any of three different *RNAis* against mitochondrial OxPhos *Complex III* (*UQCR)* or an *RNAi* against *Complex V* (*F1F0,* CG3612). Control n=34, *Complex III* (*Cyt-c1,* CG4769): *RNAi 1* (VDRC 109809) n=19, p=0.0049; *Complex III* (*UQCR-cp1,* CG3731): *RNAi 2* (VDRC 101350) n=18, p=0.024; *Complex III* (*UQCR-cp2,* CG4169): *RNAi 3* (VDRC 100818) n=16, p=0.009; *Complex V* (*F1F0, CG3612*): *RNAi* (VDRC 34664) n=21, p=0.0068. **Fig S6F-G.** Quantification of the number of macrophages in vnc segments does not show a significant change in general migration along the vnc in embryos whose macrophages express (**F**) *CV-DN* or (**G**) *RNAis* against mitochondrial OxPhos complex components compared to the control. (**F**): Control n=20, *CV-DN* n=23, p>0.05. **(G):** Control n=14, *Complex III (Cyt-c1,* CG4769): *RNAi 1* (VDRC 109809) n=10, p>0.8; *Complex III* (*UQCR-cp1,* CG3731): *RNAi 2* (VDRC 101350) n=14, p>0.05; *Complex III* (*UQCR-cp2,* CG4169): *RNAi 3* (VDRC 100818) n=11, p>0.9; *Complex V* (*F1F0,* CG3612): *RNAi* (VDRC 34664) n=18, p>0.2. Unpaired t test for (**B**) and (**D-G**).

Figure. S7

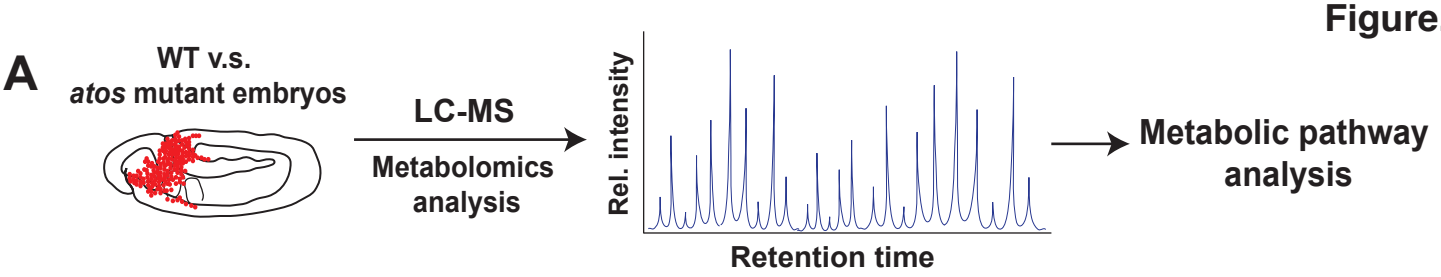

Altered metabolic pathways in *atos* embryos:
Significantly upregulated and downregulated metabolites compared to the control

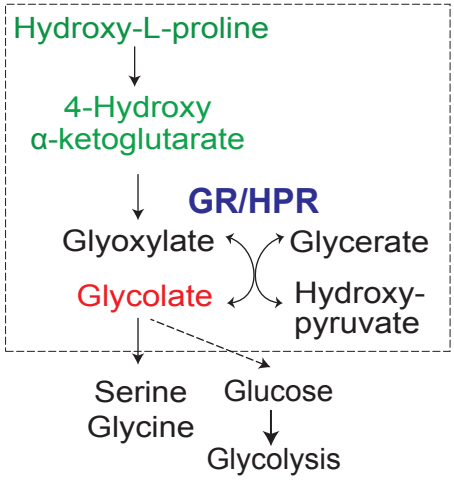

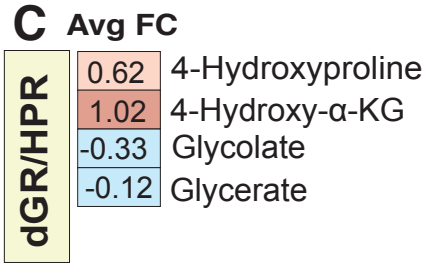

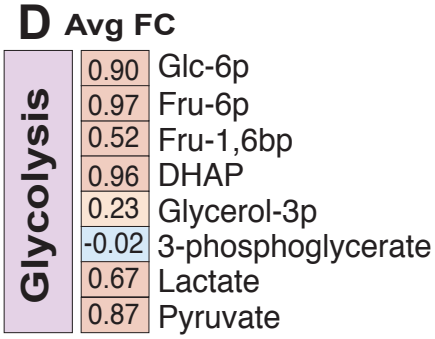

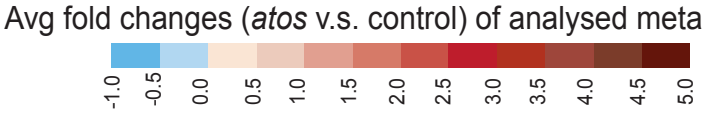

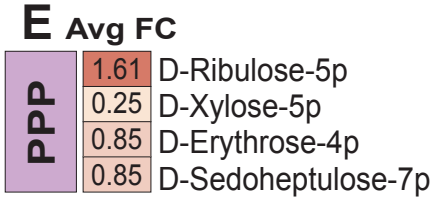

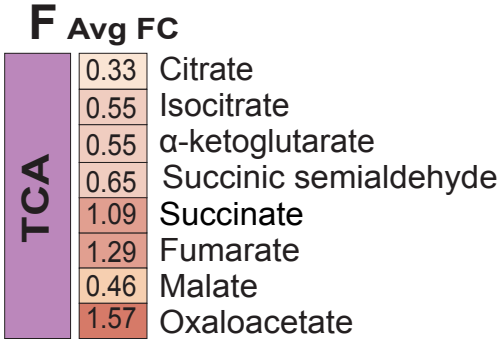

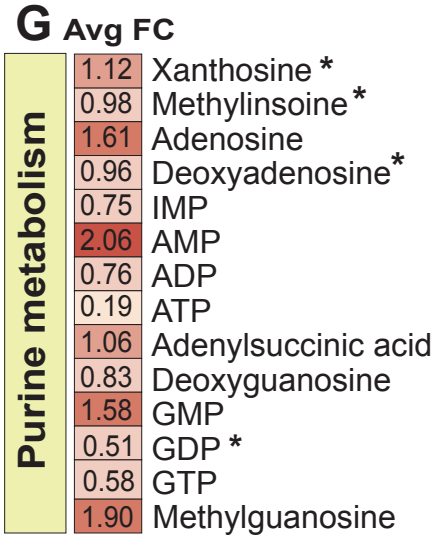

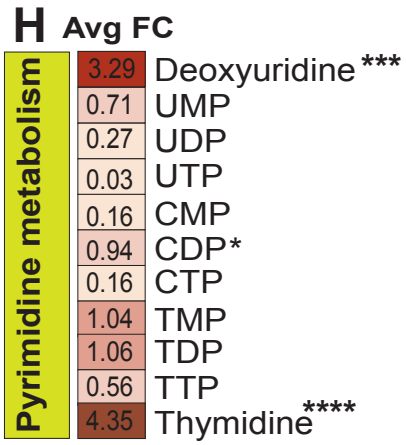

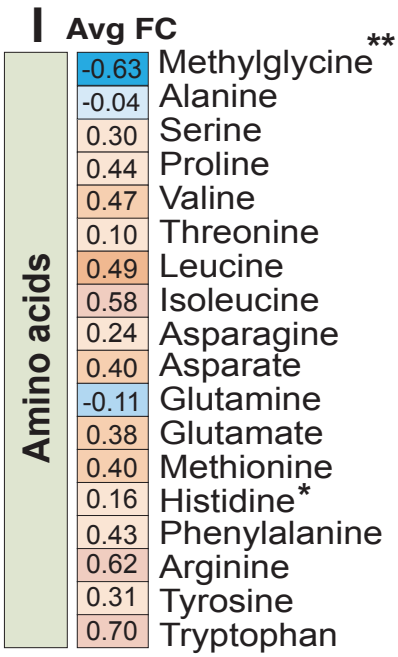

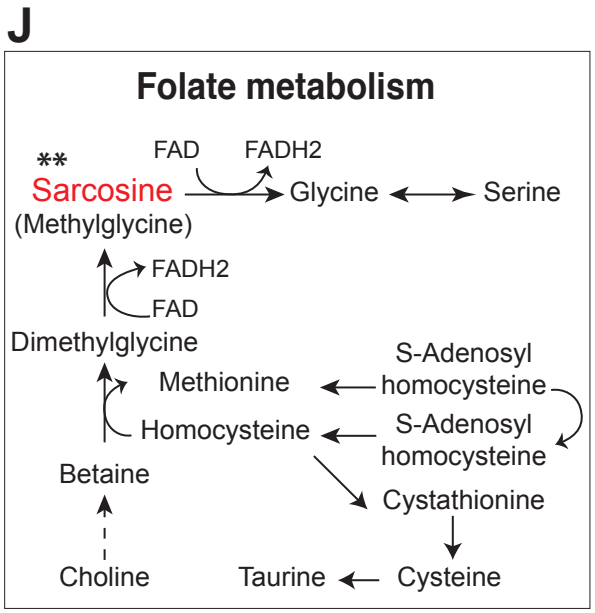

Figure S7 related to Figure 7. Atos and Porthos enhance ATP production by programming mitochondrial oxidative phosphorylation metabolism. Fig S7A. Schematic illustrates the metabolic profiling procedure in wild-type and *atos* mutant embryos at Stage 12. **Fig S7B-C.** Heatmap of non-targeted metabolites in *atos* mutant embryos reveals an increase in substrates of the dGR/HPR enzyme, including 4-hydroxy α-ketoglutarate and hydroxyproline (HLP) and a smaller decrease in its products, glycolate and glycerate. **Fig S7D-F.** Global metabolite screening reveals less than 1 fold increases for most (**D**) glycolytic intermediates and up to 3 fold increases for metabolites from (**E**) the Pentose Pathway (PPP), and (**F**) the TCA cycle in the *atos* mutant compared to the control. **Fig S7G-H.** Analysis reveals strong increases in thymidine, which can be catabolized to products that feed into the TCA cycle, as well as uridine along with increases in some cellular nucleotide precursors and purine and pyrimidine metabolites. **Fig S7I.** Heatmap of non-targeted metabolites in *atos* mutant embryos reveals a small increase in most amino acids in the *atos* mutant a significant increase in some dipeptides including those containing hydroxyproline. **Fig S7J.** Schematic shows a link between Folate metabolism and glycine/serine metabolism, in which the glycine-related metabolite sarcosine (N-methylglycine) was significantly reduced in the *atos* mutant. Metabolites with statistical significant change are shown as: *$p<0.05$, **$p<0.01$, ***$p<0.001$, ****$p<0.0001$. Unpaired t test for (**C-I**).